Fast-timing study of the l-forbidden $1/2^+ \rightarrow 3/2^+$ $M1$ transition in ^{129}Sn

R. Lică,[1,2] H. Mach,[3,*] L. M. Fraile,[4] A. Gargano,[5] M. J. G. Borge,[1,6] N. Mărginean,[2] C. O. Sotty,[2,7] V. Vedia,[4] A. N. Andreyev,[8] G. Benzoni,[9] P. Bomans,[7] R. Borcea,[2] L. Coraggio,[5] C. Costache,[2] H. De Witte,[7] F. Flavigny,[7] H. Fynbo,[10] L. P. Gaffney,[7,11] P. T. Greenlees,[12,13] L. J. Harkness-Brennan,[14] M. Huyse,[7] P. Ibáñez,[4] D. S. Judson,[14] J. Konki,[12,13] A. Korgul,[15] T. Kröll,[16] J. Kurcewicz,[1] S. Lalkovski,[17] I. Lazarus,[18] M. V. Lund,[10] M. Madurga,[1] R. Mărginean,[2] I. Marroquín,[6] C. Mihai,[2] R. E. Mihai,[2] A. I. Morales,[19,20,9] E. Nácher,[6] A. Negret,[2] R. D. Page,[14] J. Pakarinen,[12,13] S. Pascu,[2] V. Paziy,[4] A. Perea,[6] M. Pérez-Liva,[4] E. Picado,[4,21] V. Pucknell,[18] E. Rapisarda,[1] P. Rahkila,[12,13] F. Rotaru,[2] J. A. Swartz,[7] O. Tengblad,[6] P. Van Duppen,[7] M. Vidal,[4] R. Wadsworth,[8] W. B. Walters,[22] and N. Warr[23]

(IDS Collaboration)

[1]*CERN, CH-1211 Geneva 23, Switzerland*

[2]*"Horia Hulubei" National Institute of Physics and Nuclear Engineering, RO-077125 Bucharest, Romania*

[3]*National Centre for Nuclear Research, BP1, ul. Hoża 69, PL-00-681, Warsaw, Poland*

[4]*Grupo de Física Nuclear, Facultad de CC. Físicas, Universidad Complutense, CEI Moncloa, E-28040 Madrid, Spain*

[5]*Istituto Nazionale di Fisica Nucleare, Complesso Universitario di Monte S. Angelo, Via Cintia - I-80126 Napoli, Italy*

[6]*Instituto de Estructura de la Materia, CSIC, Serrano 113 bis, E-28006 Madrid, Spain*

[7]*KU Leuven, Instituut voor Kern- en Stralingsfysica, Celestijnenlaan 200D, B-3001 Leuven, Belgium*

[8]*University of York, Dept Phys, York YO10 5DD, N Yorkshire, United Kingdom*

[9]*Istituto Nazionale di Fisica Nucleare, Sezione di Milano, I-20133 Milano, Italy*

[10]*Department of Physics and Astronomy, Aarhus University, DK-8000, Aarhus C, Denmark*

[11]*School of Engineering and Computing, University of the West of Scotland, Paisley, PA1 2BE, United Kingdom*

[12]*University of Jyvaskyla, Department of Physics, P.O. Box 35, FIN-40014 University of Jyvaskyla, Finland*

[13]*Helsinki Institute of Physics, University of Helsinki, P.O. Box 64, FIN-00014 Helsinki, Finland*

[14]*Department of Physics, Oliver Lodge Laboratory, University of Liverpool, Liverpool L69 7ZE, United Kingdom*

[15]*Faculty of Physics, University of Warsaw, PL 02-093 Warszawa, Poland*

[16]*Institut für Kernphysik, Technische Universität Darmstadt, D-64289 Darmstadt, Germany*

[17]*Department of Physics, University of Surrey, Guildford GU2 7XH, United Kingdom*

[18]*STFC Daresbury, Daresbury, Warrington WA4 4AD, United Kingdom*

[19]*IFIC, CSIC-Universitat de València, E-46980 València, Spain*

[20]*Dipartimento di Fisica dell'Università degli Studi di Milano, I-20133 Milano, Italy*

[21]*Sección de Radiaciones, Universidad Nacional, Heredia, Costa Rica*

[22]*Department of Chemistry and Biochemistry, University of Maryland, College Park, Maryland 20742, USA*

[23]*Institut für Kernphysik, Universität zu Köln, Zülpicher Strasse 77, D-50937 Köln, Germany*

(Received 12 January 2016; published 4 April 2016)

The levels in ^{129}Sn populated from the β^- decay of ^{129}In isomers were investigated at the ISOLDE facility of CERN using the newly commissioned ISOLDE Decay Station (IDS). The lowest $1/2^+$ state and the $3/2^+$ ground state in ^{129}Sn are expected to have configurations dominated by the neutron $s_{1/2}$ ($l = 0$) and $d_{3/2}$ ($l = 2$) single-particle states, respectively. Consequently, these states should be connected by a somewhat slow l-forbidden $M1$ transition. Using fast-timing spectroscopy we have measured the half-life of the $1/2^+$ 315.3-keV state, $T_{1/2} =$ 19(10) ps, which corresponds to a moderately fast $M1$ transition. Shell-model calculations using the CD-Bonn effective interaction, with standard effective charges and g factors, predict a 4-ns half-life for this level. We can reconcile the shell-model calculations to the measured $T_{1/2}$ value by the renormalization of the $M1$ effective operator for neutron holes.

DOI: 10.1103/PhysRevC.93.044303

I. INTRODUCTION

Experimental information on nuclei far from the stability line is of great importance for the development of nuclear models describing the structure of nuclei at or close to the drip lines. As the N/Z ratio increases, several aspects of the effective interaction between protons and neutrons are revealed, providing unique views into the nuclear structure. In this context, the predictive power of nuclear models is subject to a stringent scrutiny, especially when the measurement of the electromagnetic transition probabilities connecting nuclear states can be achieved. These are, in fact, key observables for a reasonably fine tuning of the nuclear models.

The regions around doubly magic nuclei attract strong interest both from the point of view of experiment and theory,

[*]Deceased.

because they are the best testing ground for the shell-model effective Hamiltonian. Crucial information on single-particle energies, two-body matrix elements of the residual interaction and effective electromagnetic operators can be obtained, which can then be applied to an extended range of the nuclear chart. Nuclei in the proximity of the doubly magic ^{132}Sn ($Z=50$ and $N=82$) have a special impact, as their study provides information on the neutron-rich side of the long tin isotopic chain, which is currently known from the doubly magic ^{100}Sn up to ^{138}Sn [1].

A good description of nuclear structure around ^{132}Sn was achieved by recent realistic shell-model calculations [2], where the two-body matrix elements of the effective Hamiltonian were constructed via many-body perturbation theory, starting from a low-momentum interaction derived from the CD-Bonn nucleon-nucleon potential.

In the framework of the nuclear single-particle shell model, the magnetic dipole ($M1$) transitions are allowed only between initial and final states for which the change in orbital angular momentum is $\Delta l = 0$ [3]. Therefore, $M1$ transitions between $\Delta l = 2$ states are considered to be l forbidden, such as $s_{1/2} \leftrightarrow d_{3/2}$ and $g_{7/2} \leftrightarrow d_{5/2}$. Measurements, however, have shown that in certain cases these transitions appear to be experimentally allowed, thus providing a motivation to develop more elaborate nuclear models to understand this behavior. The breakdown of the $\Delta l = 0$ selection rule can be explained by configurational mixing [4] and/or by considering an effective $M1$ operator, resulting from the renormalization of the free operator induced by core excitations.

In the case of the ^{135}Sb system (^{132}Sn+$2n$+$1p$), for example, the B($M1$; $5/2^+ \rightarrow 7/2^+$) transition rate from the first-excited 281.7-keV level to the ground state calculated with free g factors is two orders of magnitude larger than the experimental value. This discrepancy cannot be removed by using effective g factors, but only by considering an effective $M1$ operator. This is from core-polarization effects leading to a nonzero off-diagonal matrix element of the effective $M1$ operator between the $1d_{5/2}$ and $0g_{7/2}$ proton orbitals that compensates the diagonal $0g_{7/2}$ matrix element [5,6].

An interesting case to study the l-forbidden character of $M1$ transitions is represented by the ^{129}Sn nucleus, with three-neutron holes with respect to ^{132}Sn. The low-lying state of spin $1/2^+$ at an excitation energy of 315 keV and the $3/2^+$ ground state in ^{129}Sn are expected to have configurations dominated by the neutron $2s_{1/2}$ ($l = 0$) and $1d_{3/2}$ ($l = 2$) single-particle states. These states are directly connected by a 315-keV γ transition. Because the $M1$ transition between them is most likely l forbidden and the electric quadrupole collectivity is very small for a weakly deformed nucleus, one expects a very retarded $M1$ transition from the 315-keV level to the ground state, characterized thus by a small $B(M1)$ value. The $E2$ component of the 315-keV transition should be hindered because of the single-particle nature of the states provided by the low collectivity in the region. This discussion will be continued in Sec. III.

In this paper, the half-life measurement of the second excited state of ^{129}Sn populated in the β^- decay of ^{129}In at the ISOLDE facility is reported, along with a comparison to shell-model calculations. Previous measurements of the β^- decay of ^{129}In established in great detail the level scheme of ^{129}Sn [7,8] and determined half-lives for microsecond isomers [9] which are in good agreement with shell-model calculations. Here we concentrate on the half-life of the 315-keV level, for which there are no previous experimental data available.

II. EXPERIMENTAL DETAILS

The excited states in ^{129}Sn were populated in the β decay of ^{129}In at the ISOLDE-CERN facility. A beam of ^{129}In was produced by the 1.4-GeV proton beam from the PS-Booster directly impinging on a uranium carbide (UC_x) target. The ^{129}In atoms thermally diffused out of the target matrix, were surface ionized [10], then separated using the ISOLDE General Purpose Separator (GPS) and finally brought to the center of the experimental setup at the newly commissioned ISOLDE Decay Station (IDS). IDS is positioned in a well-shielded area, more than 40 m away from the production target. The estimated ^{129}In yield was 1.2×10^4 ions/μA, and the average proton current during the run was $\sim$1 μA. Three β-decaying states coexist in ^{129}In [8]: the $J^\pi = 9/2^+$ ground state with $T_{1/2} =$ 0.61(1) s, a 459-keV isomer with $J^\pi = 1/2^-$ and $T_{1/2} =$ 1.23(3) s, and a high-lying $J^\pi = 23/2^-$ state with $T_{1/2} =$ 0.67(10) s. The corresponding 2118.3-, 315.4-, and 2189-keV transitions in ^{129}Sn which uniquely decay from each isomer were used for estimating the isomeric mixing of ^{129}In. Based on our data and the γ-ray decay intensities in the literature [8], the population of each isomeric state was found to be 56(6)%, 37(3)%, and 7(1)% for the $9/2^+$, $1/2^-$, and $23/2^-$ states, respectively.

The ^{129}In ions were implanted on the aluminium-coated Mylar transport tape at the center of the IDS, where the decay products were measured using γ and β detectors. The detection system consisted of four HPGe Clover-type detectors, two $LaBr_3$(Ce) crystals coupled to fast-timing Hamamatsu R9779 photomultiplier tubes (PMT) [11], and a thin plastic scintillator disk coupled to a fast PMT, which was employed as a fast-time response β detector. The Nutaq [12] digital data acquisition system (DAQ) was used. The Clover signals and the scintillator energy signals, taken from the PMT last dynodes, were directly fed into the DAQ. The PMT anode signals were used for the timing. The signals processed by analog constant fraction discriminators (CFD) were optimized for external delay and time walk. The processed signals were sent to time-to-amplitude converters (TAC), which were used to determine the time interval between coincident signals coming from the β and $LaBr_3$(Ce) detectors. Events were constructed offline to correlate the time differences and the detector signal amplitudes.

Energy and efficiency calibrations were performed using standard sources of ^{152}Eu, ^{133}Ba, and ^{60}Co. The time-response calibration, essential for our measurements, was obtained using a source of ^{138}Cs, which, via β decay, populates several short-lived excited states in ^{138}Ba that have well-known half-lives [13,14].

The analysis of γ–γ coincidences confirmed the ^{129}Sn level scheme reported earlier [8]. A partial level scheme which contains the main γ rays from the decay of ^{129}In isomers

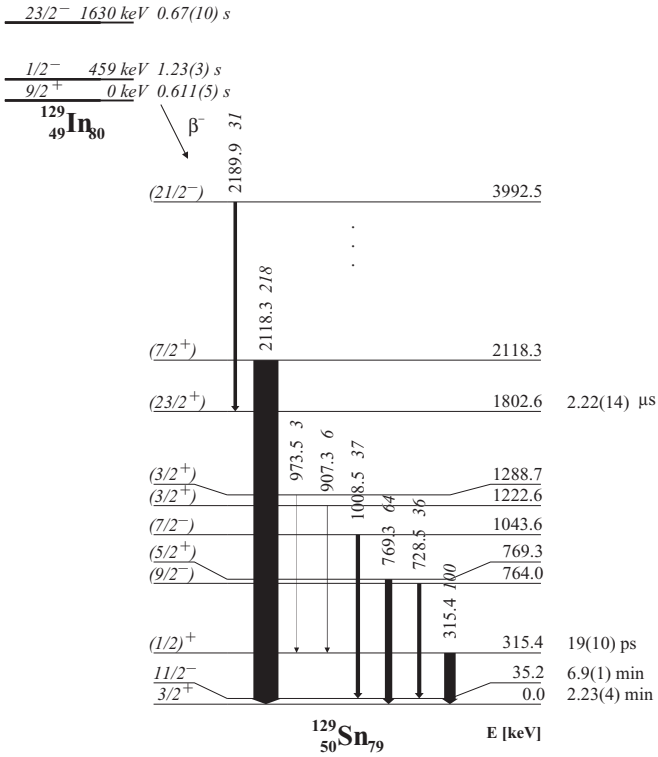

FIG. 1. Partial level scheme of ^{129}Sn [8] populated from the mixture of the three β-decaying isomers of ^{129}In indicating the γ rays relevant to the analysis. The intensities obtained in the present experiment are given relative to the 315-keV γ ray.

is shown in Fig. 1. No other new transitions could be identified and placed in the existing level scheme. The γ-ray intensities are also in agreement with Ref. [8], provided that we measured the mixture of all three isomers of ^{129}In mentioned earlier.

Figure 2 shows the β-gated $LaBr_3$(Ce) (a) and HPGe (b) summed spectra. The most intense peak corresponds to the 315-keV ($1/2^+ \rightarrow 3/2^+$) transition in ^{129}Sn. At this energy,

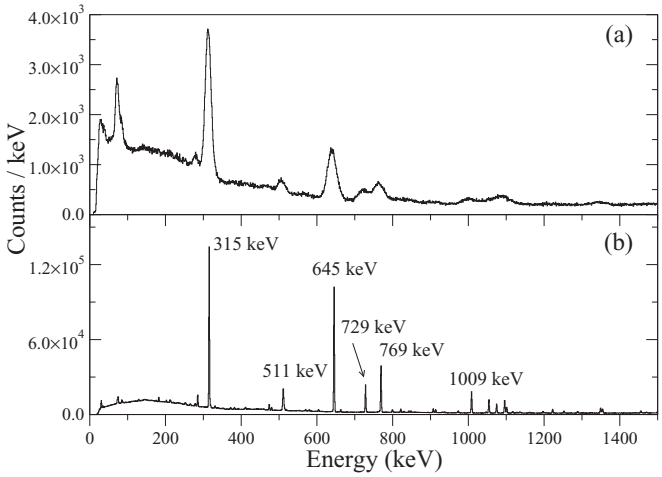

FIG. 2. β-gated γ-ray energy spectra recorded by (a) the $LaBr_3$(Ce) and (b) the HPGe γ-ray detectors. The main γ rays belong to the decay of ^{129}In. No contaminants were observed.

the full-energy peak (FEP) to background ratio is 4:1 for the HPGe and 1.5:1 for the $LaBr_3$(Ce) β-gated spectra. The intensity difference of the x rays recorded by the $LaBr_3$(Ce) and HPGe detectors is mostly from the extra thickness of the material in front of the HPGe detectors.

The half-life of the 315-keV $1/2^+$ state in ^{129}Sn was investigated by using the advanced time-delayed method (*fast timing*) for measuring nuclear half-lives in the picosecond-nanosecond range [15,16]. For very short half-lives, down to a few picoseconds, the method is based on the analytic result that the offset between the time distribution centroid and the prompt detector response is the first moment of the time distribution, and therefore it is equal to the lifetime of the exponential decay. In the case of a long half-life in the nanosecond range, the de-convolution of the decay slope can also be employed.

The time difference between β particles and γ rays was studied by analyzing the β-gated $LaBr_3$(Ce) spectra independently for both $LaBr_3$(Ce) detectors. Figure 3 shows the TAC time distribution of the 315-keV γ rays relative to the β decay. No Compton subtraction was done at this stage as the main purpose of this investigation was just exploratory to have an estimative value for the decay half-life. The time distribution shows a symmetric quasi-Gaussian response and the absence of any significant exponential decay slope rules out a lifetime in the nanosecond range. The time scale was

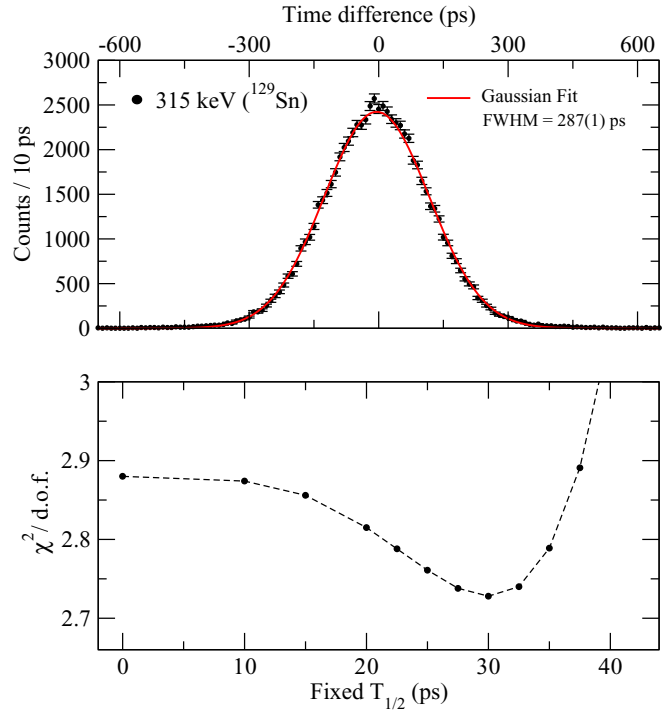

FIG. 3. The upper plot shows the time difference distribution and Gaussian fit of the 315-keV γ ray in the $LaBr_3$(Ce) detectors relative to the β particles recorded by the plastic scintillator. The Compton background is not subtracted (because of a different energy-time response of the neighboring regions) and not considered in the fit. The lower plot shows the χ^2/d.o.f. vs half-life dependence when the time distribution is fitted with a convolution of a Gaussian and an exponential function.

centered at zero for viewing purposes. The time distribution can be fitted by a Gaussian function, which suggests that the 315-keV state in ^{129}Sn has a half-life well below the time resolution of the β–LaBr$_3$(Ce) combination at this energy. The upper limit was obtained by analyzing the χ^2/d.o.f. (degrees of freedom) variation relative to the half-life when the time distribution is fitted with a convolution of a Gaussian and an exponential function. The χ^2/d.o.f. variation of < 0.1 around the minimal value suggests a half-life of 30(+7–13) ps, yielding an upper limit of ∼40 ps.

Once a long lifetime was discarded, the full analysis by the centroid-shift method was performed [15,16]. For calibration purposes, the data set containing transitions from the β decay from ^{138}Cs to ^{138}Ba [13,14] was used. Triple $\beta\gamma\gamma(t)$ events involving HPGe, LaBr$_3$(Ce), and β detectors were employed. Owing to the good energy resolution of the LaBr$_3$(Ce) detectors it was possible to select the FEP in ^{129}Sn and apply the timing corrections in double $\beta\gamma(t)$ events involving the LaBr$_3$(Ce) and β detectors. The statistics were not large enough to perform a similar $\beta\gamma\gamma(t)$ analysis. As shown in Fig. 1, the 973.5- and 907.3-keV transitions which populate the 315-keV $1/2^+$ state have low intensities.

The first step of the analysis involved the walk correction for the β detector. Although the β detector is thin and has a time response relatively independent of the incident β energy, there is still a residual time dependence that needs to be accounted for. The correction was performed relative to an intense prompt peak in the LaBr$_3$(Ce) spectra for each data set corresponding to ^{129}In. A similar treatment was done for the time calibration source of the ^{138}Cs decay.

Next, the curves representing the centroid positions of time spectrum vs γ-ray energy deposited in the LaBr$_3$(Ce) crystals [15,16] were determined both for Compton events and FEP, by using the timing information of transitions in ^{138}Ba which de-excite short-lived levels that are directly fed in the β decay of ^{138}Cs [13,14]. The transitions used as prompt reference are listed in Table I. The curves were determined using HPGe gated coincidences between the plastic scintillator and the LaBr$_3$(Ce) detectors in the triple $\beta\gamma\gamma(t)$-event data set. For the Compton walk correction an individual transition in the LaBr$_3$(Ce) detectors was selected by a suitable HPGe gate and the centroid position of the time distribution is obtained for several energy regions in the LaBr$_3$(Ce) spectra, corresponding to Compton events. The correction is used to account for the Compton time response under FEP.

TABLE I. γ-ray transitions used for determining the walk curves. Data for ^{138}Ba were taken from [13,14].

Nucleus	E_{level} (keV)	$T_{1/2}$ (ps)	E_γ (keV)	HPGe gate, (keV)
^{129}Sn	769.0		769.3	
^{129}Sb	645.1		645.2	
^{138}Ba	2307.6	7(3)	409.0	462.8
	2445.6	5(4)	138.1	871.8
			227.8	2218.0
			547.0	462.8
			1009.8	1435.8

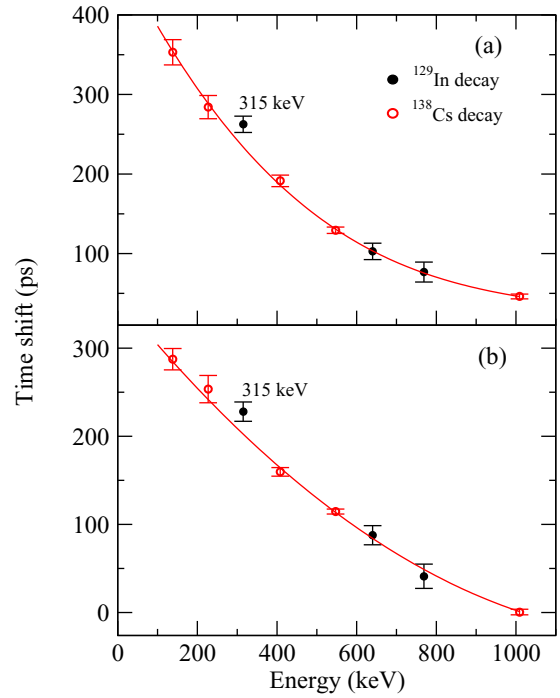

FIG. 4. The red curves correspond to the quadratic fits of the walk curves of each LaBr$_3$(Ce) detector (a) and (b), relative to the β detector. The prompt time centroids were determined using the transitions from ^{138}Ba listed in Table I. The 315-keV centroid is slightly shifted with respect to the red curve in both cases because of the lifetime of the 315-keV level.

The corrected FEP prompt response (walk) curves for the two LaBr$_3$(Ce) detectors are shown in Fig. 4. Each point represents the centroid position of the β–LaBr$_3$(Ce) FEP time distributions with the Compton background subtracted. The ^{138}Cs decay walk curve could be fitted using a quadratic polynomial thanks to the smooth time-energy response of the detectors. The 769.3-keV transition in ^{129}Sn, listed in Table I, was used as prompt reference. The 645.2-keV transition in ^{129}Sb was independently corrected for the β detector walk and used as cross-check. The time centroids in the A=129 decay chain were shifted by the same amount to match the 769.3-keV and 645.2-keV points to the curve. The difference between the centroid of the 315-keV transition and the curve is from the lifetime of the 315-keV level provided that the quadratic walk response is similar regardless of the decay chain.

The average of residuals from Fig. 4 for both LaBr$_3$(Ce) detectors is shown in Fig. 5. The reference error of ±10 ps was deduced by averaging the error bars of all the prompt γ-ray time centroids. The only statistically significant difference (offset) between the time distribution centroid and the walk curve, of $\tau = 28(15)$ ps, corresponds to the 315-keV transition. This translates into a decay half-life of $T_{1/2} = 19(10)$ ps for the 315-keV $1/2^+$ state in ^{129}Sn.

Because the experimental $M1/E2$ mixing ratio is unknown for the 315.3-keV transition, the $B(M1)$ value can be extracted as an upper limit assuming a pure $M1$ character. According to the calculations (see below) the $E2$ branch amounts to only ∼2%, therefore the $E2$ component was neglected. The 315-

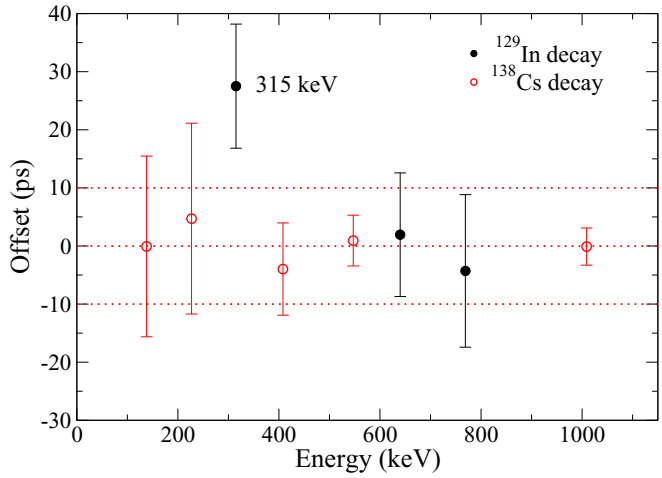

FIG. 5. Difference (offset) between each γ-ray time distribution centroid and the quadratic fit representing the walk curves shown in Fig. 4. Each point is the average of the values obtained from the two $LaBr_3$(Ce) detectors. The only point with a significant offset $\tau = 28(15)$ ps is the 315-keV centroid which translates into a half-life of $T_{1/2} = 19(10)$ ps.

keV transition from ^{129}Sn was corrected for the internal conversion, the $M1$ coefficient being 0.025 [17]. This yielded a $B(M1)$ transition rate of $6.4(30) \times 10^{-2}\ \mu_N^2 = 3.6(19) \times 10^{-2}$ W.u. indicating a relatively fast transition, contrary to the expected retarded transition.

III. THEORETICAL INTERPRETATION

With the assumption of dominant $2s_{1/2}$ and $1d_{3/2}$ configurations for the $1/2^+$ and $3/2^+$ ground state in ^{129}Sn, respectively, one would expect a small value of the $B(M1)$ transition rate between them, because of the l-forbidden nature of the Δl=2 $(2s_{1/2}-1d_{3/2})$ $M1$ transition, in contrast to our measurement of a somewhat fast transition.

To understand the properties of these two low-lying levels and the measured half-life, shell-model calculations have been performed for ^{129}Sn using a realistic two-body effective interaction. This interaction was derived [18] in the hole-hole formalism starting from the CD-Bonn potential [19], renormalized by means of the $V_{\mathrm{low-k}}$ approach with a cutoff momentum $\Lambda = 2.2$ fm^{-1}. In our calculations, ^{132}Sn is considered as a closed core with neutron holes occupying the five orbitals $0g_{7/2}$, $1d_{5/2}$, $1d_{3/2}$, $2s_{1/2}$, $0h_{11/2}$ of the 50–82 shell. The single-hole energies were taken from the experimental spectrum of ^{131}Sn. Proton and neutron excitations across the 50 and 82 shells were not explicitly included in the calculations but accounted for by the core polarization contributions to the effective interaction. Based on previous studies in the region, the matrix elements for the $J^\pi = 0^+$ channel were reduced by a factor of 0.9. More details about the derivation of the effective interaction can be found in [20]. No other adjustable parameters were needed in the calculations.

The calculated excitation energy of the yrast $1/2^+$ state is 294 keV, which is in very close agreement with the experimental value of 315 keV. Its wave-function configurations as well as those of the $3/2^+$ ground state are provided in Table II. Only configurations with a percentage $\geqslant$5% are reported for the $3/2^+$ and $1/2^+$ state, both of which are characterized by one neutron hole in the $1d_{3/2}$ and $2s_{1/2}$ orbital, respectively. It can be observed that the wave functions of both states are essentially composed of the configurations with the two remaining neutron holes in the $0h_{11/2}$ and $1d_{3/2}$ orbitals, the former being the dominant one.

TABLE II. Percentage of the wave-function configurations for the $3/2^+$ ground state and the $1/2^+$ 315-keV state in ^{129}Sn. One of the three neuron holes is always occupying the $1d_{3/2}$ and $2s_{1/2}$ orbitals in the case of the $3/2^+$ and $1/2^+$ states, respectively (see text for details).

J^π	$(nl_j)^{-2}$				
	$(0h_{11/2})^{-2}$	$(1d_{3/2})^{-2}$	$(2s_{1/2})^{-2}$	$(1d_{5/2})^{-2}$	$(0g_{7/2})^{-2}$
$3/2^+$	69%	12%	8%	6%	5%
$1/2^+$	60%	27%	7%		5%

With an effective neutron charge $e^{\mathrm{eff}} = 0.7e$ and g factors equal to $g_l^{\mathrm{free}} = 0$, $g_s = 0.7 g_s^{\mathrm{free}} = -2.68$ [20], the resulting reduced transition probabilities are $B(E2,1/2^+ \to 3/2^+) = 32.89\ e^2\mathrm{fm}^4$ and $B(M1,1/2^+ \to 3/2^+) = 0.58 \times 10^{-4}\ \mu_N^2$. Then, using the conversion coefficients 0.030 and 0.025 for the $E2$ and $M1$ transition, respectively [17], as well as the experimental excitation energy for the $1/2^+$ state, the transition probabilities $T(E2) = 0.13 \times 10^9$ s^{-1} and $T(M1) = 0.03 \times 10^9$ s^{-1} are obtained, leading to a half-life of $T_{1/2} = 4$ ns, which clearly overestimates the experimental value by two orders of magnitude.

To reconcile experiment and theory, the $\Delta l = 0$ selection rule in the $M1$ transition bare operator was relaxed by making use of an effective operator in which the core excitations are microscopically taken into account [21]. Within this approach, the calculation of the single-particle matrix elements (MEs) of this effective $M1$ operator is performed by means of many-body perturbation theory, consistently with the derivation of the effective two-body interaction including diagrams up to second order in $V_{\mathrm{low-k}}$.

The calculated effective $M1$ matrix elements are listed in Table III and compared to those obtained using g_l^{free}, $g_s = -2.68$. We see that all the new MEs are only slightly different with respect to the previous ones. However, as a major change, the off-diagonal $\Delta l = 2$ MEs becomes different from zero, and, in particular, the $\langle 1d_{3/2}||M1||2s_{1/2}\rangle$ changes from zero to $0.10\mu_N$. This result has a great relevance on the calculation of the $M1$ transition rate because of the sizable value of the corresponding one-body transition density ($\sim$0.9) as arising from the structure of the $3/2^+$ and $1/2^+$ wave functions (see Table II). In fact, with the microscopic $M1$ MEs shown in Table III, a $B(M1,1/2^+ \to 3/2^+) = 0.55 \times 10^{-2}\ \mu_N^2$ value is obtained, leading to a transition probability $T(M1) \sim 3.42 \times 10^9$ s^{-1}, which is a factor 100 larger than the one obtained with g_l^{free}, $g_s = -2.68$.

Concerning the $B(E2,1/2^+ \to 3/2^+)$, it was found that no substantial change is produced by using a microscopic effective $E2$ operator, derived within the same framework of

TABLE III. Comparison between the single-hole neutron $M1$ matrix elements (in μ_N) obtained using g factors $g_l^{\text{free}} = 0$, $g_s = -2.68$ (I), and those of the effective $M1$ operator (II) (see text for details).

a	b	$\langle a\|\|M1\|\|b\rangle_{(\text{I})}$	$\langle a\|\|M1\|\|b\rangle_{(\text{II})}$
$0g_{7/2}$	$0g_{7/2}$	1.65	1.36
$0g_{7/2}$	$1d_{5/2}$	0	0.15
$1d_{5/2}$	$1d_{5/2}$	−1.92	−1.89
$1d_{5/2}$	$1d_{3/2}$	2.05	1.88
$1d_{3/2}$	$1d_{3/2}$	1.02	1.05
$1d_{3/2}$	$2s_{1/2}$	0	0.10
$2s_{1/2}$	$2s_{1/2}$	−1.62	−1.61
$0h_{11/2}$	$0h_{11/2}$	−2.49	−2.48

the $M1$ operator. The calculated effective charge (expressed as the ME of the effective operator divided by the corresponding proton ME of the free operator) ranges from 0.8 to 1.2. The $\langle 1d_{3/2}||E2||2s_{1/2}\rangle$ ME which, as in the $M1$ case, plays a major role in the $1/2^+ \rightarrow 3/2^+$ transition, has a value of $\sim$0.8. Consequently, the $T(E2)$ increases only by a factor slightly greater than 1. It is worth noting that an enhancement of the $T(E2)$ similar to the one obtained for the $M1$ transition would require a neutron effective charge equal to 10, a value without any physical meaning.

On these grounds, we may conclude that the half-life of the $1/2^+$ state arises essentially from the $M1$ transition and, making use of the new $T(M1)$ value, becomes about 200 ps, which is still an order of magnitude larger compared to the experimental data, but clearly different from the previous calculated value indicating that the renormalization of the bare $M1$ operator induced by core-polarization effects largely contribute to the short half-life of the $1/2^+$ level in ^{129}Sn. In this context, we cannot exclude the possibility that the still existing difference between the experimental and calculated half-life may be from higher-order diagrams not included in the calculation of the $M1$ effective operator.

IV. SUMMARY AND CONCLUSIONS

The half-life of the lowest $1/2^+$ state in ^{129}Sn populated in the β^- decay of ^{129}In is reported for the first time. The measurement was carried out at the recently commissioned ISOLDE Decay Station.

The 315.3-keV $1/2^+$ state is expected to have a configuration dominated by the $\nu s_{1/2}$ single-particle orbit while the $3/2^+$ ground state is expected to be predominantly the $\nu d_{3/2}$ state. Therefore, it is expected that they are connected by a retarded l-forbidden $M1$ transition. The advanced time-delayed $\beta\gamma\gamma(t)$ fast-timing method was used to measure the 315.3-keV level half-life, yielding a value $T_{1/2} = 19(10)$ ps, and implying an enhanced transition rate of $B(M1) = 0.036(19)$ W.u.

Realistic shell-model calculations, with an effective interaction derived from the CD-Bonn nucleon-nucleon potential lead to a 4-ns half-life for the $1/2^+$ level, when standard effective charge and g factors are employed. However, by using an effective $M1$ operator derived within the same framework of the effective interaction, we calculate a half-life that is 20 times shorter, closer to the experimental value.

In conclusion, the short half-life of the $1/2^+$ level in ^{129}Sn does not necessarily imply a change in the shell structure, but can be explained as from the renormalization of the $M1$ operator.

It will be of great interest extending this investigation to the next odd Sn isotope, ^{131}Sn, the nearest neighbor below ^{132}Sn in the 50–82 shell. Furthermore, it will be important to probe the interactions for neutron particles in the 82–126 shell for ^{133}Sn, across the $N = 82$ gap.

ACKNOWLEDGMENTS

We express our deep appreciation to the late Professor Henryk Mach, who was the initiator of this investigation. He was an inspiring collaborator, mentor, and leader in developing the $\beta\gamma\gamma$(t) fast-timing technique. His memory and accomplishments will always be with us. This work was partially supported by the Spanish MINECO through Projects No. FPA2012-32443, No. FPA2013-41267-P, and CPAN Consolider (Project No. CSD-2007-00042), and by Romanian IFA Grant CERN/ISOLDE. It was also partly funded by the NuPNET network FATIMA (PRI-PIMNUP-2011-1338), by FWO-Vlaanderen (Belgium), by GOA/2010/010 (BOF KU Leuven), and by the Interuniversity Attraction Poles Programme initiated by the Belgian Science PolicyOffice (BriX network P7/12). Support from Grupo de Física Nuclear (GFN-UCM), Programmi di Ricerca Scientifica di Rilevante Interesse Nazionale (PRIN) Grant No. 2001024324 01302, German BMBF under Contracts No. 05P12PKFNE and No. 05P15PKCIA, the U.K. Science and Technology Facilities Council, and the European Union Seventh Framework through ENSAR (Contract No. 262010) is also acknowledged. Fast-timing electronics were provided by the Fast Timing Collaboration, the ISOLDE Decay Station collaboration, and MASTICON.

[1] G. S. Simpson, G. Gey, A. Jungclaus, J. Taprogge, S. Nishimura, K. Sieja, P. Doornenbal, G. Lorusso, P.-A. Söderström, T. Sumikama, Z. Y. Xu, H. Baba, F. Browne, N. Fukuda, N. Inabe, T. Isobe, H. S. Jung, D. Kameda, G. D. Kim, Y.-K. Kim, I. Kojouharov, T. Kubo, N. Kurz, Y. K. Kwon, Z. Li, H. Sakurai, H. Schaffner, Y. Shimizu, H. Suzuki, H. Takeda, Z. Vajta, H. Watanabe, J. Wu, A. Yagi, K. Yoshinaga, S. Bönig, J.-M. Daugas, F. Drouet, R. Gernhäuser, S. Ilieva, T. Kröll, A. Montaner-Pizá, K. Moschner, D. Mücher, H. Naïdja, H. Nishibata, F. Nowacki, A. Odahara, R. Orlandi, K. Steiger, and A. Wendt, Phys. Rev. Lett. **113**, 132502 (2014).

[2] L. Coraggio, A. Covello, A. Gargano, and N. Itaco, Phys. Rev. C **88**, 041304 (2013).

[3] M. G. Mayer and J. H. D. Jensen, *Elementary Theory of Nuclear Shell Structure* (John Wiley and Sons, New York, 1955).

[4] A. Arima, H. Horie, and M. Sano, Prog. Theor. Phys. **17**, 567 (1957).
[5] A. Korgul, H. Mach, B. A. Brown, A. Covello, A. Gargano, B. Fogelberg, W. Kurcewicz, E. Werner-Malento, R. Orlandi, and M. Sawicka, Eur. Phys. J. A **32**, 25 (2007).
[6] A. Covello, L. Coraggio, A. Gargano, and N. Itaco, Prog. Part. Nucl. Phys. **59**, 401 (2007).
[7] L. E. De Geer and G. B. Holm, Phys. Rev. C **22**, 2163 (1980).
[8] H. Gausemel, B. Fogelberg, T. Engeland, M. Hjorth-Jensen, P. Hoff, H. Mach, K. A. Mezilev, and J. P. Omtvedt, Phys. Rev. C **69**, 054307 (2004).
[9] J. Genevey, J. A. Pinston, H. R. Faust, R. Orlandi, A. Scherillo, G. S. Simpson, I. S. Tsekhanovich, A. Covello, A. Gargano, and W. Urban, Phys. Rev. C **67**, 054312 (2003).
[10] U. Köster, O. Arndt, E. Bouquerel, V. N. Fedoseyev, H. Frånberg, A. Joinet, C. Jost, I. S. K. Kerkines, R. Kirchner, and Targisol Collaboration, Nuclear Instruments and Methods in Physics Research B **266**, 4229 (2008).
[11] V. Vedia, H. Mach, L. M. Fraile, J. M. Udías, and S. Lalkovski, Nucl. Instrum. Methods Phys. Res., Sect. A: Accelerators, Spectrometers, Detectors and Associated Equipment **795**, 144 (2015).
[12] [http://www.nutaq.com].
[13] G. H. Carlson, W. L. Talbert, and J. R. McConnell, Phys. Rev. C **9**, 283 (1974).
[14] H. Mach and B. Fogelberg, Phys. Scr., T **56**, 270 (1995).
[15] H. Mach, R. L. Gill, and M. Moszynski, Nucl. Instrum. Methods Phys. Res., Sect. A: Accelerators, Spectrometers, Detectors and Associated Equipment **280**, 49 (1989).
[16] M. Moszynski and H. Mach, Nucl. Instrum. Methods Phys. Res., Sect. A **277** 407 (1989).
[17] T. Kibédi, T. W. Burrows, M. B. Trzhaskovskaya, P. M. Davidson, and C. W. Nestor Jr., Nucl. Instrum. Methods Phys. Res., Sect. A: Accelerators, Spectrometers, Detectors and Associated Equipment **589**, 202 (2008).
[18] L. Coraggio, A. Covello, A. Gargano, N. Itaco, and T. Kuo, Prog. Part. Nucl. Phys. **62**, 135 (2009).
[19] R. Machleidt, Phys. Rev. C **63**, 024001 (2001).
[20] M. Danchev, G. Rainovski, N. Pietralla, A. Gargano, A. Covello, C. Baktash, J. R. Beene, C. R. Bingham, A. Galindo-Uribarri, K. A. Gladnishki, C. J. Gross, V. Y. Ponomarev, D. C. Radford, L. L. Riedinger, M. Scheck, A. E. Stuchbery, J. Wambach, C.-H. Yu, and N. V. Zamfir, Phys. Rev. C **84**, 061306 (2011).
[21] P. J. Ellis and E. Osnes, Rev. Mod. Phys. **49**, 777 (1977).